Available online at
ScienceDirect
www.sciencedirect.com

Available online at www.sciencedirect.com
ScienceDirect
Fusion Engineering and Design 81 (2006) 2605–2610
Fusion Engineering and Design
www.elsevier.com/locate/fusengdes

CFD modeling of ITER cable-in-conduit superconductors Part II. Effects of spiral geometry on the central channel pressure drop

R. Zanino*, S. Giors, R. Mondino

Dipartimento di Energetica, Politecnico, I-10129 Torino, Italy

Available online 24 August 2006

Abstract

In the first paper of this series, we proposed a novel approach to help understand some of the complex processes occurring in dual-channel cable-in-conduit conductors (CICC) as used in the superconducting coils of the international thermonuclear experimental reactor (ITER): the constitutive relations including transport coefficients needed in input by standard global 1D tools for the analysis of thermal-hydraulic transients in ITER coils, e.g., the Mithrandir/M&M code, are derived from local 3D analysis. A first validation of the model was performed showing very good agreement with available experimental data from different applications. The same advanced computational fluid dynamics (CFD) tool, the FLUENT code, including sophisticated turbulence models, is used here to compute the pressure drop corresponding to an imposed mass flow rate in several geometries relevant for the central channel of the ITER CICC. The validation is extended to include more ITER-relevant conditions showing good accuracy with error bars on the friction factor $\sim\pm 15\%$. We then apply the validated model to the study of the expected dependencies of the pressure drop in the central channel of an ITER CICC on the size of the gap and on the diameter of the delimiting spiral.

Keywords: ITER; Superconducting coils; Cable-in-conduit conductors; Pressure drop; Computational fluid dynamics

1. Introduction

Dual-channel cable-in-conduit conductors (CICC) are used for the superconducting magnets of the international thermonuclear experimental reactor (ITER) [1]. Supercritical helium in forced convection at typically ~5 K and ~0.5 MPa flows both in the voids of the annular region where the cable bundle is present – a porous-medium-like structure – and in the lower-impedance central channel, delimited by a spiral. The spiral gap allows direct communication between the two regions, see Fig. 1. The assessment of the pressure drop along the CICC is crucial in the determination of the pumping cost of the coolant and its modeling requires for each region suitable friction factors. The latter ones influence also the flow repartition in the

* Corresponding author. Tel.: +39 011 564 4490; fax: +39 011 564 4499.
E-mail address: roberto.zanino@polito.it (R. Zanino).

0920-3796/$ – see front matter © 2006 Elsevier B.V. All rights reserved.
doi:10.1016/j.fusengdes.2006.07.006

Fig. 1. Build-up of a typical ITER CICC with multi-stage cable inside a circular jacket and around the central channel delimited by a spiral (central channel inner diameter $D_{in} = 10$ mm and spiral thickness $h = 1$ mm in this picture).

CICC, i.e., the fraction of flow directly available for the cooling of the cable.

Experimental efforts are being conducted worldwide to understand the thermal-hydraulics in ITER CICC and the friction issue in particular, see, e.g., [2–6]. However, notwithstanding the deceptively simple appearance of pressure drop measurements, the peculiarities of the CICC structure are such that these measurements seldom provide unambiguous results, so that the available database is today far from satisfactory [7–9].

These uncertainties motivate the development of a parallel approach in which detailed 3D CFD local analysis is used to provide constitutive relations to the global 1D computational tools currently used for superconducting coil studies like, e.g., Mithrandir/M&M [10,11]. These relations include the friction factors in the two cable regions and the heat transfer coefficients between the different cable components. Here, we concentrate on the issue of the friction factor in the central channel of an ITER CICC.

The helium flowing in the central channel sees something like a spirally rib-roughened pipe, see Fig. 2, where the gaps of the spiral are also additionally obstructed by the petal wrappings (see the thin strip wrapped around the last-but-one cabling stage in Fig. 1). Friction in the central channel was initially

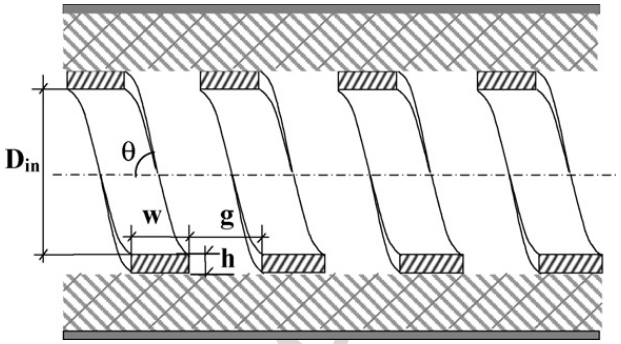

Fig. 2. Spiral geometry in an ITER CICC.

modeled using a multiplier in front of the friction factor of a smooth circular pipe [12], but it became later apparent from the increasing experimental database that both the nature of the spiral (e.g., circular spring-like versus rectangular cross-section) [4] and the gap size [3] could play a non-negligible role in determining the pressure drop. While the latter effect was also successfully correlated in Ref. [13], it should be noted that the role of the gap/thickness ratio of the spiral, g/h, on flow separation at the gap leading edge, recirculation and possible reattachment in the gap was already well-known from classical literature on compact heat exchangers [14], although typical g/h and thickness/diameter ratio, h/D, are in our case smaller and larger, respectively. Additionally, while the ITER PF coils will have a 10/12 mm ID/OD central channel, the ITER CS and TF coils will have a 7/9 mm ID/OD central channel. It becomes therefore important to try and assess also the effect of varying h/D on friction, as well as the combination of the two, i.e., is the effect of the gap size confirmed and, if so, to what extent, at smaller diameters?

The validation of the CFD approach to friction in the central channel was addressed first in Ref. [15]. Here, we study the major parametric dependencies of the friction factor on the spiral geometry, extending our previous interpretive analysis to the prediction of ITER-relevant conditions.

2. Model description

The model is based on the incompressible Navier–Stokes equations solved by the commercial FLUENT code.

As the flow in the central channel is typically turbulent, with Reynolds numbers Re in the range from 10^4 to 10^6 ($\sim 10^5$ in ITER nominal operation), the Reynolds-averaged (RANS) equations are solved and a closure is needed. Based on the previous validation [15] we adopt here the so called two-layer k–ε model [16], which proved to be more accurate than another very popular model for separated flow, namely the k–ω model, in most of the cases we considered so far. The two-layer k–ε model was also used for similar purposes in Ref. [17].

All spirals considered here have the same thickness $h = 1$ mm (common to all ITER spirals) and width $w = 6.25$ mm (a typical value for ITER spirals), while the gap g and the diameters D_{in}, D_{out} ($=D_{\text{in}} + 2h$) vary. Only one pitch length ($= w + g$) of the spiral is considered, under the assumption of fully developed flow, according to which the local pressure gradient can be decomposed into the gradient of a periodic component + the constant gradient of a linearly varying component [18]. The computational domain includes only the central channel and gaps, taking advantage of the fact that the spiral + the petal wraps constitute an effective, almost impermeable wall for the flow. Therefore, at steady state (equilibrium) hardly any interaction with the flow in the annular region occurs, which is assumed to justify our simplifying hypothesis. Note that the independence of the two flows (annular region and central channel) is also implicitly assumed in the customary interpretation of experimental data, see below.

The finite volume grid is made of hexahedra in the region close to the spiral/wall, then moving to tetrahedra in the core flow region, in order to avoid excessive distortion because of the spiral geometry [15]. The typical number of volumes/cells ranges between a few 10^5 up to $\sim 10^6$ or so, depending on the different geometries and Reynolds number. In the most critical cases, numerical convergence (grid independence) was verified. For instance, simulation of the so-called I10 spiral ($g = 7.29$ mm, $D_{\text{in}} = 8$ mm), at given mass flow rate ($Re = 9.2 \times 10^4$), gave $f = 0.01421$ using ~ 0.250 Mcells ("coarse mesh") and $f = 0.01427$ using ~ 0.580 Mcells ("fine mesh"); simulation of the central channel of the so-called CS1.2B conductor (Showa spiral with $g = 2.7$ mm, $D_{\text{in}} = 10$ mm), at given pressure gradient = 60 kPa/m, gave $Re \sim 5.7 \times 10^4$ ($f = 0.0128$) with ~ 0.650 Mcells and $Re \sim 5.6 \times 10^4$ ($f = 0.0133$) with ~ 1.17 Mcells. At higher Re the mesh requirements increase as expected: for the Showa spiral at $Re = 5 \times 10^5$ we get $f = 0.0074$ using ~ 0.250 Mcells and $f = 0.0096$ using ~ 0.600 Mcells, so that a finer mesh is mandatory in these cases. Finally, particularly at large g/h the solution accuracy benefits of a suitable alignment of the grid in the gap to the directions along the gap and orthogonal to the wall, respectively ("aligned mesh").

The fluid used in the simulations is always H_2O but hydrodynamic similarity was verified by comparison with a simulation using N_2 (both at RT). Consequently, these results can be applied to the cryogenic conditions we are interested in by translation from pressure drop Δp versus mass flow rate ($\mathrm{d}m/\mathrm{d}t$) to dimensionless form $f(Re)$, according to the formulas:

$$Re = \frac{\mathrm{d}m}{\mathrm{d}t}\frac{D_{\text{h}}}{\mu A}$$

$$f = \frac{1/2(\Delta p/L)\rho D_{\text{h}} A^2}{(\mathrm{d}m/\mathrm{d}t)^2}$$

where μ is the constant fluid dynamic viscosity, L the reference (test section) length, ρ the fluid density and we choose $D_{\text{h}} = D_{\text{in}}$ as the hydraulic diameter, $A = \pi D_{\text{in}}^2/4$ as the flow area.

3. Results and discussion

We have parametrically analyzed a relevant sub-set of the cases of present and future ITER relevance, scanning the g/h and the h/D parameter space according to Fig. 3.

In view of the considerations made in the introduction, the two major questions we are trying to answer in this paper are the following:

(1) Is the g/h effect (increasing f for increasing but sufficiently low g/h), which was measured at "large" D_{in}, confirmed also at "low" D_{in}?
(2) Is there an h/D effect, i.e., is f dependent on h/D at given Re and g/h?

3.1. Effect of g/h at different D_{in}

We will first check if the simulations are able to reproduce the g/h effect measured at $D_{\text{in}} = 10$ mm,

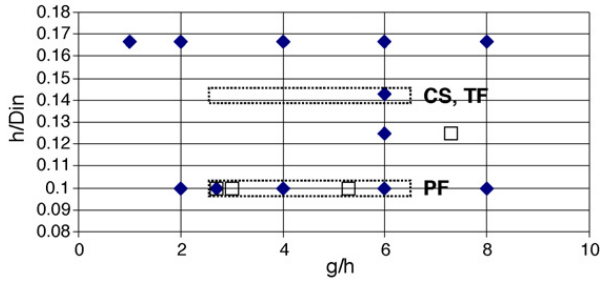

Fig. 3. Parameter space considered in the present study. Solid symbols, simulations; open symbols, experimental data available; dashed rectangles, range of respective ITER coils.

and then consider the situation in the limit case $D_{in} = 6$ mm.

Fig. 4 shows the validation and convergence of the simulations at $g = 2.7$ mm and $D_{in} = 10$ mm. It appears that over a broad range of Re (10^4 to 5×10^5) experimental data on different fluids (H_2O in the CS1.2B conductor at low Re [2], N_2 at high Re in a rubber or SS pipe with Showa spiral insert [13,19]) can be reasonably reproduced by the simulations. At $Re \geq 5 \times 10^4$ the measured f is underestimated by the simulations, as already observed in Ref. [17] for a similar, albeit 2D case, with a maximum error of the order of ~15% when a fine mesh is used, while the opposite happens at low Re. Runs performed on a relatively coarse mesh (~0.25 Mcells), further underestimate the computed friction factor, see Fig. 4, but the trend of the results is the same as with the fine mesh, so that *we shall use mainly coarse meshes in the following parametric studies, which have mainly qualitative purpose*.

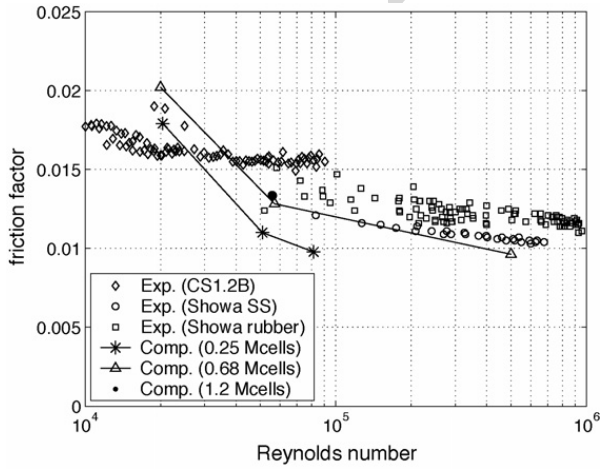

Fig. 4. Validation and convergence at $g = 2.7$ mm and $D_{in} = 10$ mm.

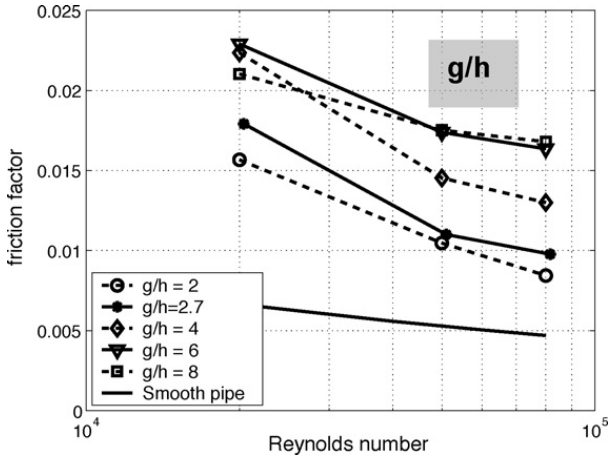

Fig. 5. Parametric study of g/h effect at $D_{in} = 10$ mm.

Fig. 5 shows the result of the parametric study on the effect of g/h at different Re for $D_{in} = 10$ mm. It is seen that the well-known (at least for 2D conditions) non-monotonic trend of f with g/h [20] is confirmed by our 3D simulations at low Re. Note that the non-monotonicity may be easily understood by observing that both $g/h \to 0$ and $g/h \to \infty$ correspond to a smooth tube limit.

If we consider the case of $D_{in} = 6$ mm, see Fig. 6, while $g/h = 6$ again corresponds to maximum f (even at low Re, as confirmed by a convergence run not shown) the sensitivity of f to g/h is weaker (at $Re = 8 \times 10^4$ and for g/h going from 2 to 6, $\Delta f/f \sim 50\%$ versus ~100% for $D_{in} = 6$ mm versus 10 mm).

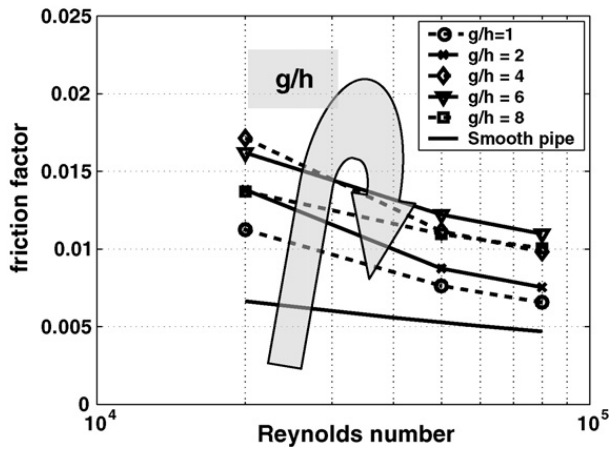

Fig. 6. Parametric study of g/h effect at $D_{in} = 6$ mm.

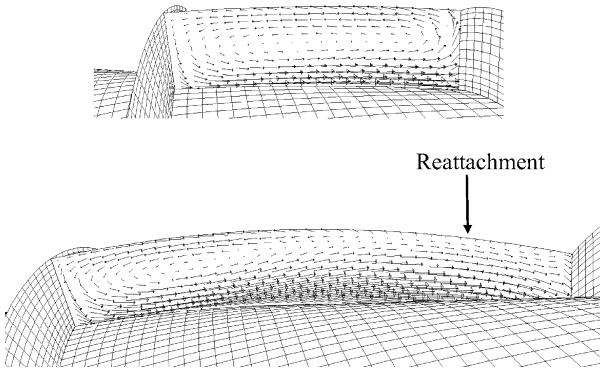

Fig. 7. Computed velocity field on a surface orthogonal to the gap edges (see text) at $Re = 2 \times 10^4$ and $D_{in} = 6$ mm: (top) $g/h = 4$ and (bottom) $g/h = 8$.

In order to try and understand the effect of g/h in 3D we show in Fig. 7 a comparison between computed velocity fields on a surface orthogonal to the gap edges and normal to the local helicoidal direction χ at the "bottom" of the gap. Indeed, it is seen that a recirculation vortex without reattachment appears in the gap at g/h below the maximum f, while at g/h above the maximum f the flow reattaches to the "bottom" of the gap, as in 2D geometries [14].

This qualitative picture is quantitatively confirmed in Fig. 8 by the plot of the normalized shear stress ($C_f = \tau_w/(1/2\rho V^2)$, $V = (dm/dt)/\rho A$), along the intersection between the "bottom" of the gap and the above

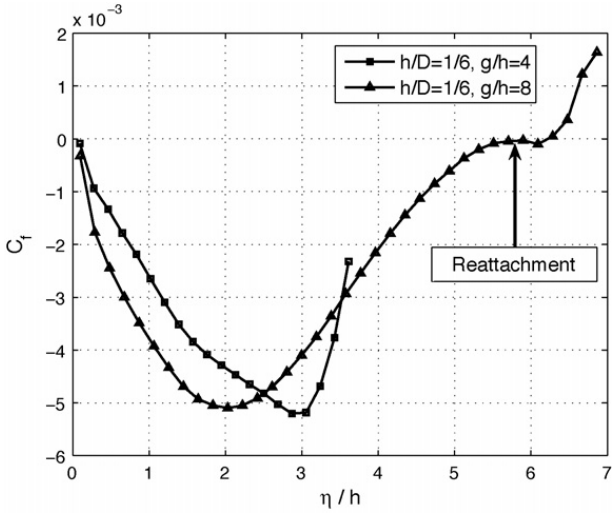

Fig. 8. Comparison of computed shear stress at wall for $Re = 2 \times 10^4$ and $D_{in} = 6$ mm, for different g/h, vs. curvilinear coordinate η normal to χ (see text).

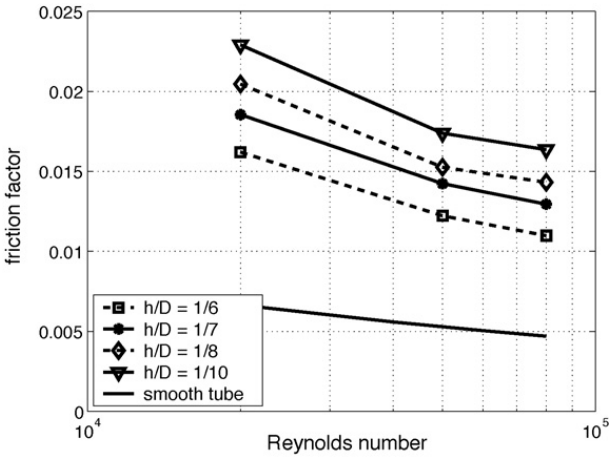

Fig. 9. Parametric study of h/D effect at $g/h = 6$.

surface, if we recall that C_f goes to zero at reattachment.

3.2. Effect of h/D at given Re and g/h

The effect of h/D was investigated at fixed $g/h = 6$ and is shown in Fig. 9 (for 2D ribs a similar behavior at different g/h obtains, not shown). It is seen that a decreasing f is computed at increasing h/D and given Re. This somewhat counterintuitive effect of the "relative roughness" has to do with the fact that the friction factor at given dm/dt or given Re scales as $\Delta p D^5$ or $\Delta p D^3$, respectively. While Δp obviously decreases, at given (dm/dt), when D increases, the increase of D can offset the reduction of Δp. Indeed, if D_{out} was used (for both D_h and A) in the definition of Re instead of D_{in}, the effect would reverse, with increasing h/D leading to increasing f at given Re, showing some ambiguity in the h/D dependence of f at given Re and g/h. Note that, at much lower h/D than considered here, f increases with h/D [14], but this can be qualitatively understood because the reduction of D is too small to compensate the increase of Δp.

4. Conclusions and perspective

CFD provides a very useful tool for the detailed local analysis of thermal-hydraulic phenomena in ITER CICC. Validation of this approach to the problem of friction in the central channel was started in Ref. [15] and has been continued here, showing good agreement

between simulations and experiment over a broad range of operating conditions.

The major parametric effects of spiral geometry have been simulated with the following results:

- The (initially) increasing f with g/h measured at $D_{in} = 10$ mm [13] is reproduced by the model. A similar (although quantitatively smaller) sensitivity is anticipated by the simulations at smaller D_{in}. Roughly independently of D_{in} and Re, f reaches a broad maximum for $g/h \sim 6$. Therefore, either sufficiently smaller or sufficiently larger g/h should be chosen for ITER CICC, at least for the purpose of minimizing the pressure drop, while room of optimization still exists under the complete set of constraints (including heat and mass transfer between the two regions, mechanical stiffness of the spiral for manufacturing purposes, etc.).
- The g/h dependence of f is due to the flow pattern in the gap, with reattachment of the flow at the "bottom" of the gap playing the major role in determining the maximum friction even in 3D, as it was well-known in 2D geometries.
- An h/D dependence of f is predicted by the simulations, but it is rather ambiguous as it may reverse depending on the choice of diameter (D_{in} versus D_{out}) used in the definition of Re.

In perspective, a full set of simulation results on very fine meshes will be used to derive a general correlation for f (Re, g/h, h/D).

References

[1] P. Komarek, Results of magnet tests as a basis for the design of ITER magnets, Fus. Eng. Des. 74 (2005) 77–85.

[2] P. Bruzzone, Pressure drop and helium inlet in the ITER CS1 conductor, Fus. Eng. Des. 58–59 (2001) 211–215.

[3] S. Nicollet, J.L. Duchateau, H. Fillunger, R. Heller, R. Maix, L. Savoldi, et al., Hydraulic resistance of the ITER toroidal field model coil dual channel cable-in-conduit conductor pancake, in: Proceedings of the 19th International Cryogenic Engineering Conference (ICEC19), 2002, pp. 161–164.

[4] K. Hamada, T. Kato, K. Kawano, E. Hara, T. Ando, H. Tsuji, et al., Experimental results of pressure drop measurements in ITER CS model coil tests, Adv. Cryo. Eng. 47 (2002) 407–414.

[5] R. Zanino, C.Y. Gung, K. Hamada, L. Savoldi, Pressure drop analysis in the CS insert coil, Adv. Cryo. Eng. 47 (2002) 364–371.

[6] C. Marinucci, P. Bruzzone, A. dellaCorte, L. Savoldi Richard, R. Zanino, Pressure drop of the ITER PFCI cable-in-conduit conductor, IEEE Trans. Appl. Supercond. 15 (2005) 1383–1386.

[7] R. Zanino, L. Savoldi Richard, A review of thermal-hydraulic issues in ITER cable-in-conduit conductors, Cryogenics 46 (2006) 541–555.

[8] R. Zanino, P. Bruzzone, L. Savoldi Richard, A critical assessment of pressure drop design criteria for the conductors of the ITER magnets, Adv. Cryo. Eng. 51 (2006) 1765–1772.

[9] R. Zanino, L. Savoldi Richard, Task TW1-TMC CODES design and interpretation codes. Del. 1a. Part 1. Investigation on flow characteristics (analysis of pressure drop tests in OTHELLO), April 2005 (unpublished).

[10] R. Zanino, S. DePalo, L. Bottura, A two-fluid code for the thermohydraulic transient analysis of CICC superconducting magnets, J. Fus. Energy 14 (1995) 25–40.

[11] L. Savoldi, R. Zanino, M&M: multi-conductor Mithrandir code for the simulation of thermal-hydraulic transients in superconducting magnets, Cryogenics 40 (2000) 179–189.

[12] K. Hamada, Y. Takahashi, N. Koizumi, H. Tsuji, A. Anghel, B. Blau, et al., Thermal and hydraulic measurement in the ITER QUELL experiments, Adv. Cryo. Eng. 43 (1998) 197–204.

[13] R. Zanino, P. Santagati, L. Savoldi, A. Martinez, S. Nicollet, Friction factor correlation with application to the central cooling channel of cable-in-conduit super-conductors for fusion magnets, IEEE Trans. Appl. Supercond. 10 (2000) 1066–1069.

[14] R.L. Webb, E.R.G. Eckert, R.J. Goldstein, Heat transfer and friction in tubes with repeated-rib roughness, Int. J. Heat Mass Transfer 14 (1971) 601–613.

[15] R. Zanino, S. Giors, R. Mondino, CFD modeling of ITER cable-in-conduit super-conductors. Part I. Friction in the central channel, Adv. Cryo. Eng. 51 (2006) 1009–1016.

[16] H.C. Chen, V.C. Patel, Near-wall turbulence models for complex flows including separation, AIAA J. 26 (1988) 641–648.

[17] B. Arman, T.J. Rabas, Two-layer model predictions of heat transfer inside enhanced tubes, Numer. Heat Transfer A 25 (1994) 721–741.

[18] S.V. Patankar, C.H. Liu, E.M. Sparrow, Fully developed flow and heat transfer in ducts having streamwise-periodic variations of cross-sectional area, ASME J. Heat Transfer 99 (1977) 180–186.

[19] S. Nicollet, J.L. Duchateau, Task CODES: results of ITER type central spirals friction factor measurements in the OTHELLO facility and application for ITER Coils, CEA Report AIM/NTT-2003.018, 2003.

[20] J.C. Han, L.R. Glicksman, W.M. Rohsenow, An investigation of heat transfer and friction for rib-roughened surfaces, Int. J. Heat Mass Transfer 21 (1978) 1143–1156.